Transactions of the Korean Nuclear Society Autumn Meeting
Gyeongju, Korea, October 29-30, 2015

Microtomography with a sandwich detector for mouse bone imaging

Seung Ho Kim [a], Hanbean Youn[b,c], Junwoo Kim[a], Hosang Jeon[b,c], Ho Kyung Kim [a,c*]
[a]*School of Mechanical Engineering, Pusan National University, Busan, South Korea*
[b]*Department of Radiation Oncology, Pusan National University Yangsan Hospital, Yangsan, Kyungsangnam-do, South Korea*
[c]*Center for Advanced Medical Engineering Research, Pusan National University, Busan, South Korea*
[*]*Corresponding author: hokyung@pusan.ac.kr*

1. Introduction

Dual-energy imaging can remove overlapping anatomical structures that obscure the detection of lesions by discriminating the material content. And single-shot dual-energy imaging, using sandwich detector, the rear detector usually uses a thicker x-ray converter to enhance quantum efficiency with the higher-energy spectrum, hence providing a blurrier image than the front detector. The weighted logarithmic subtraction of the two images therefore results in a form of unsharp masking that enhances edges in the resultant image. Inspired by this observation, we have developed a micro computed tomography (micro-CT) system with the sandwich detector for high-resolution bone imaging of small animals. The sandwich detector consists of two flat-panel detectors by stacking one upon the other. Although the x-ray beam continuously irradiates, the step-rotation of an object and stay-readout of projection data were considered for the scanning and data gathering.

2. Material and Methods

As shown in Fig. 2, we have developed a bench-top micro-CT system with the sandwich detector. During continuous x-ray irradiation, the object rotates on its axis by an amount of prescribed step angle and then the rotation stays until the sandwich detector produces two projection images. These motion and image readout are computer-controlled and last till a single rotation completes. The distances from the x-ray focal spot to the detector and from the focal spot to the axis of rotation are computer-controlled variables. The pixel pitch of the detector is 0.048 mm, and the magnification of the pixel pitch of the rear detector is negligible. The active area of the sandwich detector is dependent upon the size of the CMOS photodiode array used: ~25×50 mm^2. We prepared a postmortem mouse phantom (~40 g) by replacing blood by paraformaldehyde.

Bone-enhanced images of the mouse phantom may be obtained from two different ways: image reconstruction with bone-enhanced projection data and bone-enhancing subtraction of reconstructed images with the respective projection data obtained from the front and rear detectors. These two methods may be respectively described as follows:

$$f_{bone}(\mathbf{r}) = \mathbf{FBP}\{-\mathbf{w}\mathbf{p}_F + \mathbf{p}_R\} \quad (1)$$

and

$$f_{bone}(\mathbf{r}) = -w\mathbf{FBP}\{\mathbf{p}_F\} + \mathbf{FBP}\{\mathbf{p}_R\}, \quad (2)$$

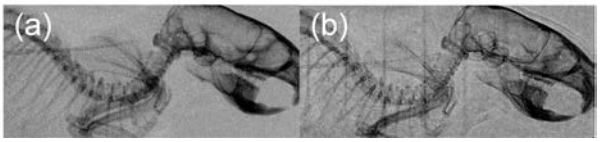

Figure 1. Comparison of dual-energy postmortem mouse images obtained from (a) dual-shot (40/70 kVp switching) and (b) single-shot (using the sandwich detector at 70 kVp) methods

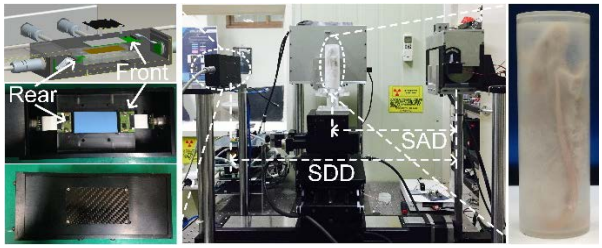

Figure 2. A picture describing the micro-CT system. The enlarged views show the sandwich detector and a postmortem mouse phantom.

where $\mathbf{p}_j$ denotes the projection data obtained from the jth detector layer. w denotes the weighting factor and $\mathbf{w}$ implies a diagonal matrix consisting of weighting factors corresponding to each projection. The operator $\mathbf{FBP}\{\cdots\}$ implies the filtered backprojection operation and we used the FDK algorithm[3] with the Hann filter. Hereafter, we call the two methods the "projection-" and "image-based" bone-enhancing methods, respectively. To obtain bone-enhanced projections or reconstructed images, we used the weighted logarithmic subtraction approach. The optimal weighting factor for logarithmic subtraction can be determined by minimizing contrast between the material to be subtracted and background. In the projection-based bone-enhancing dual-energy CT, we applied the same weighting factor to all the projections for convenience.

3. Preliminary results

Figure 3 shows the sample projection images of the mouse head obtained at the system magnification ratio of 1.5 with the x-ray spectrum from the tungsten-anode operated at 50 kVp.

Reconstructed sample images are shown in Fig. 4. The axial image obtained from the front detector with a thin scintillator shows streak artifacts around high-density bone regions whereas that from the rear detector with a thicker scintillator shows less streak artifacts. However, the spatial resolution performance is poor in the axial image with the rear detector. Although the soft-tissue information is absent, the projection-based bone-enhancing method produces an axial image with clear bone details. In addition, the streak artifacts

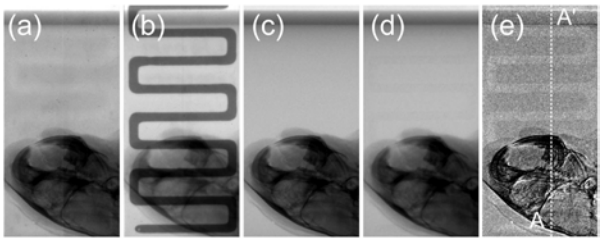

Figure 3. Sample projection images. (a) and (b) are images obtained from the front and rear detectors, repectively. (c) and (d) are preprocessed images of (a) and (b), respectively. The corresponding dual-energy image is shown in (e).

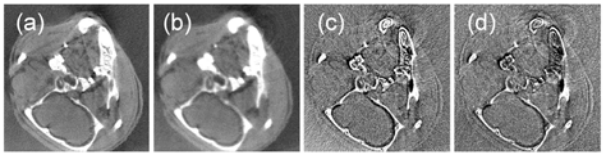

Figure 4. Axial images along the A-A' line as shown in Fig. 3 (e): (a) and (b) are the reconstructed images with projections obtained from the front and rear detectors, respectively. (c) is the reconstructed image with bone-enhanced projections. (d) is the weighted logarithmic subtraction between (a) and (b).

are negligible. We note that the projection-based method outperforms the image-based method. All images were displayed with the level of their mean value and a window of two times their standard deviations.

4. Further study

It will be necessary that more elaborate experiments with the mouse and/or other quantitative phantoms. And quantification of the image quality of bone-enhanced images in comparisons with the conventional images will be performed. The image analysis of differences between bone-enhanced images obtained from the projection- and image-based approaches can be performed.

ACKNOWLEDGMENTS

"This work was supported by the National Research Foundation of Korea (NRF) grant funded by the Korea government (MSIP) (No. 2013M2A2A9046313)."

REFERENCES

[1] S. Yun, J. C. Han, D. W. Kim, H. Youn, H. K. Kim, J. Tanguay, and I. A. Cunningham, "Feasibility of active sandwich detectors for single-shot dual-energy imaging," 2014.

[2] J. C. Han, H. K. Kim, D. W. Kim, S. Yun, H. Youn, S. Kam, J. Tanguay, and I. A. Cunningham, "Single-shot dual-energy x-ray imaging with a flat-panel sandwich detector for preclinical imaging," *Current Applied Physics* **14**(12), pp. 1734–1742, 2014.

[3] L. A. Feldkamp, L. C. Davis, and J. W. Kress, "Practical cone-beam algorithm," *J. Opt. Soc. Am. A* **1**, pp. 612–619, Jun 1984.